REPORT DOCUMENTATION PAGE

Form Approved
OMB No. 0704-0188

1. REPORT DATE (DD-MM-YYYY) 05-09-2005	2. REPORT TYPE REPRINT	3. DATES COVERED (From - To)

4. TITLE AND SUBTITLE
Remote Sensing of Gravity Wave Intensity and Temperature Signatures at Mesopause Heights Using the Nightglow Emissions

5a. CONTRACT NUMBER

5b. GRANT NUMBER

5c. PROGRAM ELEMENT NUMBER
62601F

6. AUTHOR(S)
M.J. Taylor[1], W.R. Pendleton, Jr.[1], S.H. Seo[1], and R. H. Picard[2]

5d. PROJECT NUMBER
2301

5e. TASK NUMBER
BD

5f. WORK UNIT NUMBER
A1

7. PERFORMING ORGANIZATION NAME(S) AND ADDRESS(ES)

Air Force Research Laboratory
29 Randolph Road
Hanscom AFB, MA 01731-3010

8. PERFORMING ORGANIZATION REPORT NUMBER

AFRL-VS-HA-TR-2005-1117

9. SPONSORING / MONITORING AGENCY NAME(S) AND ADDRESS(ES)

10. SPONSOR/MONITOR'S ACRONYM(S)

AFRL/VSBYB

11. SPONSOR/MONITOR'S REPORT NUMBER(S)

12. DISTRIBUTION / AVAILABILITY STATEMENT
Approved for Public Release; Distribution Unlimited.

[1] Utah University, Logan UT   [2] Air Force Research Laboratory, Hanscom AFB, MA

13. SUPPLEMENTARY NOTES
Reprinted from: Proceedings of SPIE Vol. 4882 (2003), Pages 122 - 133

14. ABSTRACT

During the past four decades a variety of optical remote sensing techniques have revealed a rich spectrum of wave activity in the upper atmosphere. Many of these perturbations, with periodicites ranging from ~5 min to several hours and horizontal scales of a few ten's of km to several thousands km, are due to freely propagating buoyancy (or acoustic- gravity waves), and forced tidal oscillations. Optical observations of the spatial and temporal characteristics of these waves in the mesosphere and lower thermosphere (MLT) region (~80-100 km) are facilitated by several naturally occurring, vertically distinct nightglow layers. This paper describes the use of state-of-the-art ground-based CCD imaging techniques to detect these waves in intensity and temperature. All-sky (180') image measurements from Bear Lake Observatory, Utah are used to illustrate the characteristics of small-scale, short period (< 1 hour) waves that are most frequently observed at MLT heights including a particular set of ducted wave motions, possibly associated with mesospheric bores. These results are then contrasted with measurements of mesospheric temperature made using a separate imaging system capable of determining induced temperature amplitudes of much larger-scale wave motions and investigating night-to-night and seasonal variability in mesospheric temperature.

15. SUBJECT TERMS

Atmospheric gravity waves Thermosphere	Mesosphere Nightglow	Temperature remote sensing

16. SECURITY CLASSIFICATION OF:

a. REPORT UNCLAS	b. ABSTRACT UNCLAS	c. THIS PAGE UNCLAS	17. LIMITATION OF ABSTRACT SAR	18. NUMBER OF PAGES 12	19a. NAME OF RESPONSIBLE PERSON Richard H. Picard
					19b. TELEPHONE NUMBER (include area code) 781-377-2222

Standard Form 298 (Rev. 8-98)
Prescribed by ANSI Std. 239.18

Remote Sensing of Gravity Wave Intensity and Temperature Signatures at Mesopause Heights Using the Nightglow Emissions

M.J. Taylor[*a], W.R. Pendleton, Jr.[a], S.H. Seo[a], and R. H. Picard[b]

[a]Center for Atmospheric and Space Science and Physics Department, Utah State University, Logan, UT 84321, USA; [b]Air Force Research Laboratory, Space Vehicles Directorate, Hanscom AFB, Bedford, MA 01731-3010, USA

ABSTRACT

During the past four decades a variety of optical remote sensing techniques have revealed a rich spectrum of wave activity in the upper atmosphere. Many of these perturbations, with periodicites ranging from ~5 min to several hours and horizontal scales of a few ten's of km to several thousands km, are due to freely propagating buoyancy (or acoustic-gravity waves), and forced tidal oscillations. Optical observations of the spatial and temporal characteristics of these waves in the mesosphere and lower thermosphere (MLT) region (~80-100 km) are facilitated by several naturally occurring, vertically distinct nightglow layers. This paper describes the use of state-of-the-art ground-based CCD imaging techniques to detect these waves in intensity and temperature. All-sky (180°) image measurements from Bear Lake Observatory, Utah are used to illustrate the characteristics of small-scale, short period (< 1 hour) waves that are most frequently observed at MLT heights including a particular set of ducted wave motions, possibly associated with mesospheric bores. These results are then contrasted with measurements of mesospheric temperature made using a separate imaging system capable of determining induced temperature amplitudes of much larger-scale wave motions and investigating night-to-night and seasonal variability in mesospheric temperature.
Keywords: Atmospheric gravity waves, mesosphere, thermosphere, nightglow, temperature remote sensing

1. INTRODUCTION

Thermal tides and planetary waves appear to dominate the motion fields in the mesosphere and lower thermosphere (MLT) region (~80-100 km) due to their large horizontal and vertical amplitudes. However, current knowledge suggests that the largest systematic influence on the MLT region results from the much smaller-scale freely propagating gravity waves because of their ability to transport significant amounts of energy and momentum up from the lower atmosphere to the MLT region where they influence the mean wind and the larger-scale wave motions. As these short-period waves steepen due to adiabatic wave growth with altitude (or by reaching critical layers), they deposit their energy and momentum. In so doing they give rise to horizontal motions, which act to oppose the background flow and produce closure of the mesospheric jet [e.g. [1-4]], as well as vertical motions resulting in strong adiabatic cooling responsible for the unexpectedly cold summer mesopause at polar latitudes (as much as 90 K below the radiative equilibrium level). Thus, gravity waves, in particular small-scale waves [e.g. [5]] are now understood to be a key element in defining both the large-scale circulation, and the regional thermal structure and dynamical variability of the atmosphere at altitudes extending from the stratosphere into the MLT region.

To help quantify the effects of gravity waves at MLT heights their spatial and temporal characteristics, geographic distribution and seasonal variability are of key interest. However, as the mean winds and tides in the intervening atmosphere can modulate the gravity wave fluxes, and as they both vary strongly with latitude and season, the upward flux of waves (and hence momentum) at a given site and time is expected to vary significantly. Nevertheless, this variation in not yet known for *any* place on earth. The TIMED satellite mission, launched 7 December 2001, is

---
[*] mtaylor@cc.usu.edu; phone 1-435-797-3919; fax 1-435-713-0054; Center for Atmospheric and Space Science and Physics Department, Utah State University, Logan, UT 84321, USA.

Remote Sensing of Gravity Wave Intensity and Temperature Signatures at Mesopause Heights Using the Nightglow Emissions

M.J. Taylor[*a], W.R. Pendleton, Jr.[a], S.H. Seo[a], and R. H. Picard[b]

[a]Center for Atmospheric and Space Science and Physics Department, Utah State University, Logan, UT 84321, USA; [b]Air Force Research Laboratory, Space Vehicles Directorate, Hanscom AFB, Bedford, MA 01731-3010, USA

ABSTRACT

During the past four decades a variety of optical remote sensing techniques have revealed a rich spectrum of wave activity in the upper atmosphere. Many of these perturbations, with periodicites ranging from ~5 min to several hours and horizontal scales of a few ten's of km to several thousands km, are due to freely propagating buoyancy (or acoustic-gravity waves), and forced tidal oscillations. Optical observations of the spatial and temporal characteristics of these waves in the mesosphere and lower thermosphere (MLT) region (~80-100 km) are facilitated by several naturally occurring, vertically distinct nightglow layers. This paper describes the use of state-of-the-art ground-based CCD imaging techniques to detect these waves in intensity and temperature. All-sky (180°) image measurements from Bear Lake Observatory, Utah are used to illustrate the characteristics of small-scale, short period (< 1 hour) waves that are most frequently observed at MLT heights including a particular set of ducted wave motions, possibly associated with mesospheric bores. These results are then contrasted with measurements of mesospheric temperature made using a separate imaging system capable of determining induced temperature amplitudes of much larger-scale wave motions and investigating night-to-night and seasonal variability in mesospheric temperature.

Keywords: Atmospheric gravity waves, mesosphere, thermosphere, nightglow, temperature remote sensing

1. INTRODUCTION

Thermal tides and planetary waves appear to dominate the motion fields in the mesosphere and lower thermosphere (MLT) region (~80-100 km) due to their large horizontal and vertical amplitudes. However, current knowledge suggests that the largest systematic influence on the MLT region results from the much smaller-scale freely propagating gravity waves because of their ability to transport significant amounts of energy and momentum up from the lower atmosphere to the MLT region where they influence the mean wind and the larger-scale wave motions. As these short-period waves steepen due to adiabatic wave growth with altitude (or by reaching critical layers), they deposit their energy and momentum. In so doing they give rise to horizontal motions, which act to oppose the background flow and produce closure of the mesospheric jet [e.g. 1-4], as well as vertical motions resulting in strong adiabatic cooling responsible for the unexpectedly cold summer mesopause at polar latitudes (as much as 90 K below the radiative equilibrium level). Thus, gravity waves, in particular small-scale waves [e.g. 5] are now understood to be a key element in defining both the large-scale circulation, and the regional thermal structure and dynamical variability of the atmosphere at altitudes extending from the stratosphere into the MLT region.

To help quantify the effects of gravity waves at MLT heights their spatial and temporal characteristics, geographic distribution and seasonal variability are of key interest. However, as the mean winds and tides in the intervening atmosphere can modulate the gravity wave fluxes, and as they both vary strongly with latitude and season, the upward flux of waves (and hence momentum) at a given site and time is expected to vary significantly. Nevertheless, this variation in not yet known for *any* place on earth. The TIMED satellite mission, launched 7 December 2001, is

[*] mtaylor@cc.usu.edu; phone 1-435-797-3919; fax 1-435-713-0054; Center for Atmospheric and Space Science and Physics Department, Utah State University, Logan, UT 84321, USA.

dedicated to investigating the basic structure and large-scale variability of the MLT region (up to 180 km). However, due to the temporal and spatial averaging inherent in the TIMED mission, there is no on-board instrumentation capable of measuring the spectrum of small-scale gravity waves. In contrast, the coordinated use of ground-based measurements with TIMED (as part of a collaborative program between NASA and the U.S. National Science Foundation [NSF]), together with existing ground-based data sets provides an extremely important resource for investigating the role of gravity waves on MLT dynamics.

Of equal importance is the investigation of the properties of the MLT region (background temperature and wind fields) in which the waves propagate and dissipate. Measurements using powerful Na wind-temperature lidar systems have provided unprecedented information on the vertical structuring of the MLT and the influence of tides on it [e.g. 6]. Furthermore, Na lidar data have provided a basic climatology of the MLT temperature variability at mid-latitudes [7]. However, due to their complexity lidar systems are usually operated only 2-3 nights/month. The resultant climatology therefore lacks necessary details associated with spring and fall transitions (from winter to summer, and vice-versa) and short-term variability due to planetary waves, tides and gravity waves.

In this paper we present example measurements of small-scale gravity waves remotely sensed in the MLT nightglow emissions to illustrate their characteristics and variability. We include new measurements on a class of frontal phenomena in the mesosphere with associated waves whose characteristics resemble undular bores.[8] The data were obtained using an all-sky, monochromatic imaging system capable of detecting gravity waves in the visible and near-infrared (NIR) nightglow emissions.[9, 10] These data are then contrasted with a series of measurements obtained by a separate state-of-the art imaging system designed specifically to investigate mesospheric temperature and its variability with high precision on a near-nightly basis.

2. IMAGING SMALL SCALE-GRAVITY WAVES

Images of the naturally occurring nightglow emissions afford an excellent method for investigating the horizontal morphology and dynamics of short-period (typically <1 hour) gravity waves. There are several prominent emissions at MLT heights which can be used for this study: the NIR OH bands (peak altitude ~87 km), the $O_2(0,1)$ Atmospheric band (~94 km), the OI(557.7 nm) green line (~96 km) and the Na D (589.2 nm) doublet (~90 km), all of which exhibit typical nighttime halfwidths (FWHM) of 8-10 km. As gravity waves propagate through these layers they induce significant modulation in the line-of-sight brightness and rotational temperature which is detected as radiance "structure". Several instruments have been developed to investigate the morphology and dynamics of the nightglow emissions. However, the exceptional capabilities of high quantum efficiency CCD arrays for low-light imaging studies at visible and NIR wavelengths makes them the detectors of choice for many gravity wave studies. In particular, all-sky (180°) imagers provide unique two-dimensional information on the spatial and the temporal properties of short-period gravity waves (~5-60 min) over a maximum (single site) area of ~500,000 km^2 [e.g. 9-15].

Imaging systems are most sensitive to relatively fast-moving waves exhibiting vertical wavelengths somewhat greater than the layer thickness (i.e. >8 km) and horizontal wavelengths (λ_h) ~5-200 km (i.e. significantly less than the maximum field of view). This is exactly the range of scale sizes that are the most important drivers of the MLT region dynamics.[16] These small-scale waves exhibit vertical group velocities (of a few 10's m/s) and can propagate rapidly from their source regions into the MLT. The majority of these waves (λ_h up to a few hundred km) are considered to be generated in the lower atmosphere by weather related disturbances such as convective activity, wind shear instabilities (jet streams), storms or fronts, or by orographic forcing (wind flow over mountainous regions).

Image measurements of the airglow emissions can be made at any latitude and season providing a global, all year round capability. Such studies have revealed a wealth of small-scale wave activity at equatorial, mid- and high latitudes from many sites around the world and it is not uncommon to observe several different wave patterns during the course of a night suggesting copious sources. Figure 1 illustrates a variety of wave patterns that are most commonly observed in the MLT emissions. These observations have mainly been made from mid- and low latitude mountain sites and distinct spatial and temporal properties have emerged which suggest the existence of two dominant types of short-period waves, termed "bands" and "ripples" (akin to those seen in noctilucent clouds). Figure 1a illustrates in OI the most

prominent quasi-monochromatic pattern which usually appears as an extensive, coherent series of waves that exhibit horizontal wavelengths of a few to several tens of kilometers and horizontal phase speeds up to 100 ms^{-1}. Such band displays are persistent, usually lasting for a few to several hours, and are spatially extensive, often occupying an area of sky much larger than the instantaneous all-sky field of view. In this image the bands appear as a series of curved waves (like the segments of an orange), due to the distortion by the all-sky lens. However, when they are mapped into geographic coordinates they often (but certainly not always) appear as an extensive series of quasi-plane waves. Indeed, in this example the wave pattern appeared nearly linear and exhibited a horizontal wavelength of 38 ± 2 km, and on observed phase speed of 34 ± 3 ms^{-1}, indicating an observed period of 19 ± 2 min. Band-type wave patterns have been shown to be due to freely propagating or ducted buoyancy waves, most probably of tropospheric origin.

In contrast, the second type of wave motion (termed ripples) is quite distinct from the bands, exhibiting much smaller spatial and temporal scales. Ripples usually occur in localized wave packets that occupy much smaller regions of the sky, typically <5 x 10^3 km^2. They have relatively short lifetimes (a few minutes to ~ 45 min) and almost always exhibit periods close to the local Brunt-Väisälä period (~5 min). Two ripple patterns are also evident in Figure 1a superimposed on the band-type wave pattern. A likely source of ripples is the chance combinations of wind and long-period wave motions (including tides) creating localized regions of strong wind shear which then generate small-scale waves *in situ* through the Kelvin-Helmholtz instability.[17] Alternatively, the waves may be generated by a three-dimensional convective instability, in which case the waves should form near orthogonal to the perturbing wave [e.g. [15]]. In each case the wave pattern will be short-lived and spatially localized, as evident in the image data.
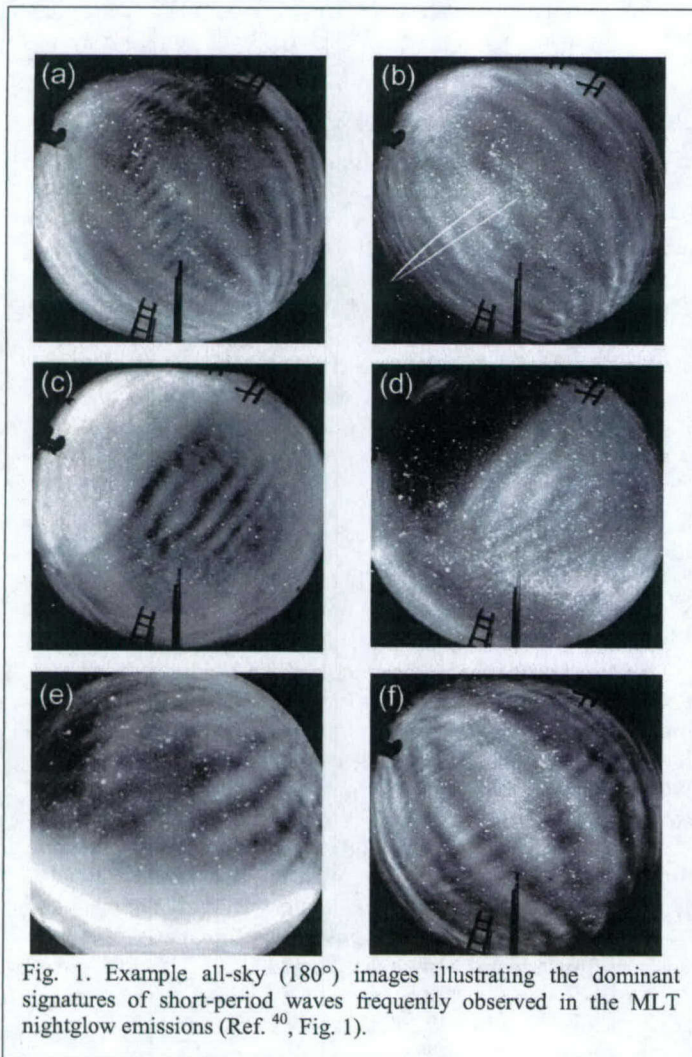

Fig. 1. Example all-sky (180°) images illustrating the dominant signatures of short-period waves frequently observed in the MLT nightglow emissions (Ref. [40], Fig. 1).

The importance of multi-layer measurements is illustrated in Figure 1b which shows the wave structure imaged in the Na emission layer at approximately the same time as Figure 1a. (Note that the bright lines are due to a Na lidar beam probing two regions of sky during the 120 sec image exposure.) The same band pattern is clearly evident in this emission (and in the OH and O$_2$ emissions) indicating that this wave motion was coherent and extended vertically throughout the MLT region whereas the ripples are absent revealing their limited horizontal and vertical extent.

Figure 1e shows another example of band-type wave structure (λ_h = 35.5 ± 1.0 km) but this time imaged in the high-latitude (~65°N) OH emission from central Alaska. The bright arc in the lower part of the image is due to auroral precipitation. Joule heating and other forcing associated with solar-induced magnetic storms are a known source of large-scale buoyancy waves that are often detected in the high altitude ionosphere as travelling ionospheric disturbances (TIDs). However, in this case the bands were moving towards the auroral zone suggesting other, tropospheric-type sources.

Finally, Figure 1c,d show a different class of band-type motion that we have termed a "frontal event". Unlike most band patterns this type of wave is characterized by a sharp leading edge followed by a discrete number (typically <10) of trailing wave crests, similar in morphology to an undular bore on a river. This transient type of wave pattern, accompanied by a dc level change, is much less common than the banded patterns and is thought to be the signature of a mesospheric bore accompanied by trapped (or ducted) wave propagating near horizontally at mesospheric heights (see Section 4). Such bores and the associated waves propagate near the mesopause temperature minimum in ducts formed by temperature and wind structure. In this case the contrast reversal evident in the two images (OI left; OH right), indicates that the effect of the bore intrusion on the airglow layers was to simultaneously decrease the height of the lower NIR OH layer and raise the upper OI (557.7 nm) layer.[18]

These examples have been chosen for their simplicity and ability to illustrate the variety of short-period wave motions that exist at MLT heights. However, at any one time there may be many more waves evident, resulting in a complex, time-varying airglow pattern. Such a situation is shown in the OI (557.7 nm) image of Figure 1f. In this case two band-type motions progressing in almost orthogonal directions are evident. The temporal evolution of these events reveals the true, exceptionally dynamic nature of the MLT region.

The histogram plots of Figure 2 illustrate the range of values typically observed for bands. In this case the data were obtained from a site close to the equator in northern Brazil.[19] Since January 2000 we have obtained year round data (typically 18 nights/month centered on new moon) from Bear Lake Observatory (41.6°N, 111.6°W) as part of our "baseline" studies for the TIMED satellite mission which was launched in December 2001. These observations form part of a coordinated set of "image chain" measurements across the Rocky Mountain, with additional imagers located at Grand Junction, Colorado (S. B. Mende, University California at Berkeley), Socorro, New Mexico (G. R. Swenson, University of Illinois) and Ft. Collins, Colorado (L. Kieffaber, Whitworth College), providing a simple but powerful method of obtaining systematic data on small-scale wave dynamics over an exceptionally large geographic area ($>10^6$ km^2) in conjunction with the TIMED satellite measurements.

3. INVESTIGATING WAVE ANISOTROPY

A common result arising from airglow image analysis is that the waves often exhibit marked preference in their propagation headings over a period of a few weeks. Such measurements made over the course of a year are quite rare but indicate strong anisotropy that varies systematically with the seasons. Taylor et al.[20] were the first to investigate this anisotropy in image data and attributed it to wave blocking by winds. Their results, obtained over a 3-month period from Ft. Collins, Colorado, indicate that critical-layer filtering of the waves by the background winds in the intervening atmosphere (stratosphere and lower mesosphere) was an important factor in governing the propagation of wave energy into the MLT region. Critical layers occur when the horizontal wind vector along the direction of motion of the wave equals its observed horizontal phase speed [e.g. [21]]. Under these conditions the intrinsic frequency of the gravity wave is Doppler-shifted to zero and its energy may be absorbed into the background flow.
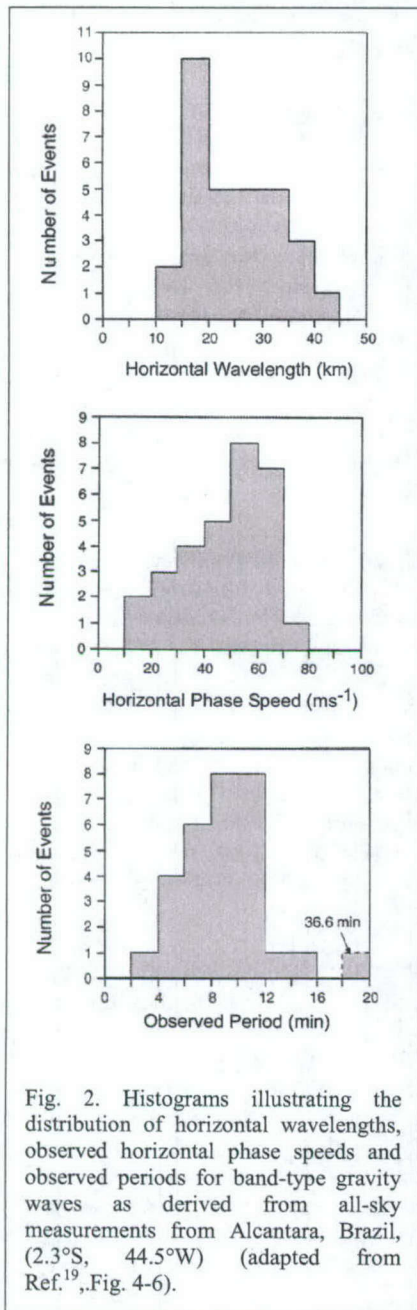

Fig. 2. Histograms illustrating the distribution of horizontal wavelengths, observed horizontal phase speeds and observed periods for band-type gravity waves as derived from all-sky measurements from Alcantara, Brazil, (2.3°S, 44.5°W) (adapted from Ref.[19],.Fig. 4-6).

Figure 3 shows the results of a 1-year investigation of all-sky OH wave data imaged from Cacheoira Paulista, Brazil (23°S). The measurements have been divided into the four seasons with the observed directionality plotted as a function of the observed wave speed. (Note that the data have been divided into four months each for winter and summer and two months each for the spring and autumn transition periods.) It is clear that during the course of the year the direction of the waves switches over from eastward in the summer months to westward in the winter months.[22] This result is consistent with the reversal of the stratospheric winds, whose magnitudes are comparable to the wave phase speeds, and suggests that the small-scale gravity wave flux is being modulated strongly by the middle atmospheric winds. This situation is indicated by the shaded areas that represent height-integrated "blocking regions". These are forbidden regions for the waves resulting from wind filtering at lower altitudes [e.g. [20]] and were constructed using CIRA-86 climatological wind profiles. The prevailing direction of the wave ensemble is clearly opposite to that of the height-integrated blocking region. Such climatological/model computations may be performed for each airglow emission (OH, Na, O_2, OI) altitude and are an important tool for studying the effects of wave filtering by the winds between the tropospheric source region and the MLT airglow layer.[22]
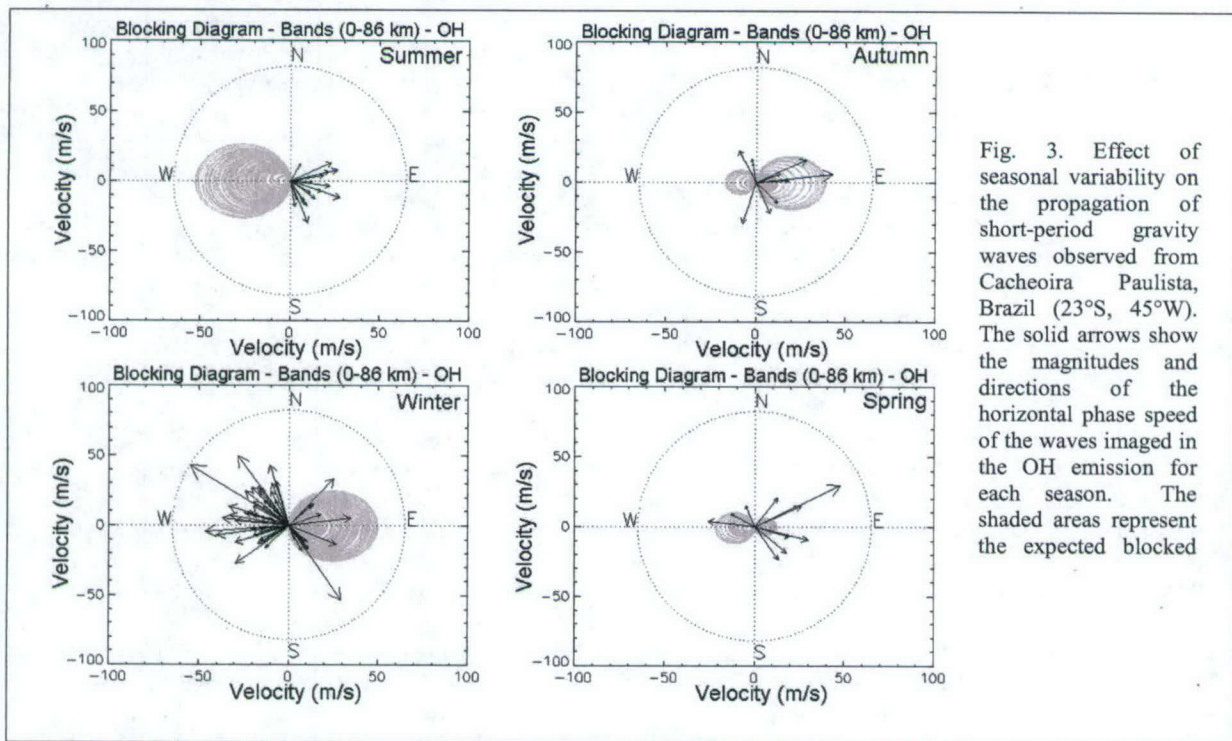

Fig. 3. Effect of seasonal variability on the propagation of short-period gravity waves observed from Cacheoira Paulista, Brazil (23°S, 45°W). The solid arrows show the magnitudes and directions of the horizontal phase speed of the waves imaged in the OH emission for each season. The shaded areas represent the expected blocked

Other observers have also reported anisotropy in their wave measurements [e.g. [23-25]]. In some cases the observed anisotropy is suggestive of wave ducting rather than wind filtering. Ducting can occur due to shears in the background winds in the MLT region (termed Doppler ducting) or to changes in the local temperature gradient (termed thermal or Brunt ducting). Due to their relatively small scale sizes short-period waves are susceptible to both thermal and Doppler ducting in the vicinity of the mesopause [e.g. [26, 27]]. Unlike freely propagating waves, ducted waves can travel large horizontal distances from their source regions. An analysis of the image data obtained during the ALOHA-93 Campaign indicated that as much as 75% of the waves imaged over the mid-Pacific ocean (during spring 1993) exhibited ducted or evanescent characteristics due to Doppler ducting effects.[28] More recently, Walterscheid et al.[24] and Hecht et al.[25] have shown that thermal ducting may be responsible for the strong directionality observed in short-period wave propagation over southern Australia and south-eastern USA.
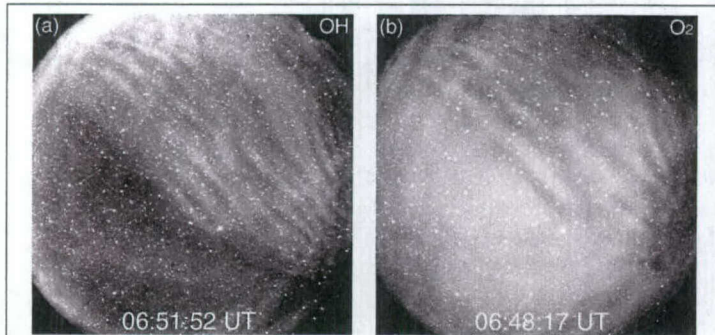
4. MESOSPHERIC FRONTS / UNDULAR BORES

Fig. 4. Two example images illustrating a mesospheric frontal event imaged near-simultaneously in the NIR OH and the O_2 Atmospheric band from Bear Lake Observatory, Utah (41.6°N, 111.6°W). Note the similarity between this image pair and the frontal event shown in Fig. 1c,d.

Figure 4 shows two example all-sky images of the same gravity wave pattern detected near-simultaneously in the NIR OH and the O_2 (0,1) band emissions from Bear Lake Observatory (BLO), (41.6°N, 111.6°W). The data were recorded on 26/27 April 2000 and together with the low-latitude (20.8° N, 156°W) images of Figure 1c,d they illustrate the distinctive coherent signature of mesospheric front events [e.g. [11]]. In this case the associated wave train extended from horizon to horizon and exhibited a horizontal wavelength of ~30 km and an observed period of ~10 min (compared with 19 km and 4.2 min for the event in Figure 1c,d). The duration of these unusual events is typically a few hours. Following their first identification[11] in 1993 over the Hawaiian Islands, Seo[8] performed a preliminary investigation of the occurrence and characteristics of mid-latitude frontal events using extensive data available from BLO. A total of 29 months of data spanning the period 1994-1997 were visually inspected for the presence of frontal events yielding 16 well-defined displays (with a number of other possible, but lower contrast events). By far the highest number of events (12) occurred during the extended summer months from May to September, with the remaining 4 events occurring in January and February. No events were observed during the early spring (March and April) and during the late autumn/early winter months, October, November and December. However, the number of events investigated is currently too few to ascribe any clear trend to their occurrence frequency.

To illustrate the variability in these events, Table 1 lists the principal characteristics of seven frontal displays as measured in the OH emission. Simultaneous measurements of each event were made in at least two airglow emissions. The mean values for the OH and OI data were found to be: horizontal wavelength λ_h = 15-18 km, horizontal phase speed V_h ~47 m/s and observed period τ_{ob} ~6-7 min. The largest variability occurred in the horizontal phase speed which ranged from 15-75 m/s but with a clear preference for relatively fast observed phase speeds of >40 m/s. The azimuthal information shows several of these events propagating from the north but their sources have yet to be investigated.

Table 1. Example measurements of the wave characteristics associated with seven mesospheric front displays imaged in the OH emission from Bear Lake Observatory during the period 1994-1996. A total of 16 events were recorded during this period.

UT Date	λ_h (km)	V_h (m/s)	τ_{ob} (min)	Azimuth (±5°)
21 Jan 1994	22.1 ± 1.5	52 ± 1	7.2	183°
4 May 1994	10.4± 0.1	60± 1	2.9	129°
4 May 1995	15.1 ±0.4	46± 1	5.5	102°
1 Sept. 1995	22.2± 0.5	41 ±2	9.0	358°
23 Jan 1996	25.8± 0.2	72± 3	5.3	178°
23 June 1996	12.4± 0.5	42± 1	4.9	7°
1 July 1997	15.5± 0.6	42± 2	6.2	25°

Example traces of two of the events listed in Table 1 (4 May 1994 and 23 June 1996) showing the frontal brightness profiles taken in a direction orthogonal to the front are presented in Figure 5. These traces illustrate cases where the OH and OI image brightness variations (1) are 180° out of phase (as in Figure 1c,d), exhibiting a clear contrast reversal as observed in the original ALOHA-93 Campaign observation[11] (Figure 5a,b), and (2) are in phase (i.e. no contrast reversal evident) (Figure 5c,d). Notice that both the front (dc brightness level change) and the associated waves show

this phase behavior in each case. According to the interpretation of these mesospheric frontal events as undular bores,[18, 29] the bore creates a transient phase disturbance propagating in a wave duct that may be formed by either temperature-inversion layers and/or by wind-shear regions at the airglow layer altitudes. Using this interpretation we can attribute the differing intensity curves of Figure 5a,b to a bore occurring in the altitude region between the two airglow layers which will give opposite phase brightness variations, while a bore occurring beneath the two layers will lead to in-phase brightness variations (Fig. 5c,d).
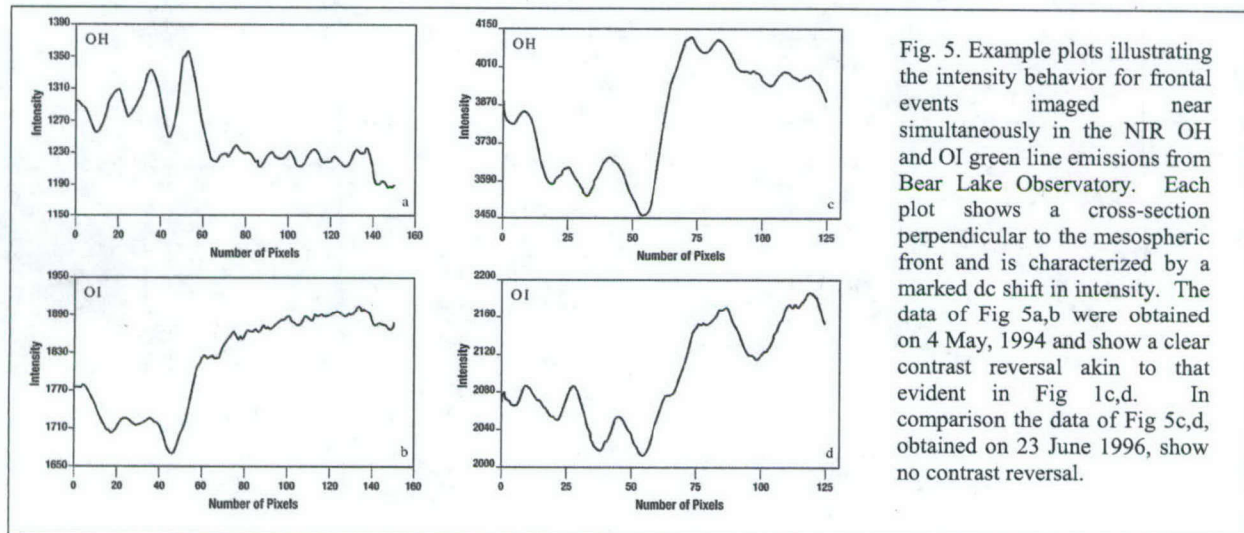

Fig. 5. Example plots illustrating the intensity behavior for frontal events imaged near simultaneously in the NIR OH and OI green line emissions from Bear Lake Observatory. Each plot shows a cross-section perpendicular to the mesospheric front and is characterized by a marked dc shift in intensity. The data of Fig 5a,b were obtained on 4 May, 1994 and show a clear contrast reversal akin to that evident in Fig 1c,d. In comparison the data of Fig 5c,d, obtained on 23 June 1996, show no contrast reversal.

5. GRAVITY WAVE TEMPERATURE PERTURBATIONS

The Mesospheric Temperature Mapper (MTM) was developed at Utah State University as part of the NSF CEDAR Phase III initiative for new instruments for upper atmospheric research. The system utilizes a state-of-the-art digital camera which incorporates a high quantum efficiency (~50% at NIR wavelengths) bare 1024x1024 pixel CCD array. The large dynamic range and low noise characteristics (dark current ~0.1 el/pixel/sec at −50° C) of this array together with its high linearity and stability provide an exceptional capability for long-term, quantitative measurements of the nightglow emissions. The camera has a 75° field of view and is fitted with a fast (f/5.6) telecentric lens system permitting narrow-band ($\Delta\lambda \cong 1.2$ nm) measurements of the OH Meinel (6,2) $P_1(2)$ and $P_1(4)$ rotational lines to investigate the mesospheric temperature and intensity perturbations at ~87 km altitude. To attain the large S/N ratios required for precise (better than 2K in 3 min) temperature determinations, the image data are binned on chip from the original format down to 128 x 128 superpixels resulting in a zenithal footprint of about 0.9 km x 0.9 km. This resolution is similar to that used by Hecht et al.[15] and is quite sufficient to resolve even the shortest scale gravity waves ($\lambda_h > 5$km) [e.g. [17]].

In operation, three sequential one-minute exposures are made using filters with center wavelengths of 840 nm [$P_1(2)$ Λ-doublet], 846.5 nm [$P_1(4)$ Λ-doublet], and 857 nm (background) for each temperature measurement, resulting in an effective sampling rate of $\cong 18$ hr^{-1}. Rotational temperatures are computed using the ratio method, described by Meriwether[30] for the (8,3) band. A value 1.300 has been adopted for the ratio of transition probabilities, A[$P_1(4)$] / A[$P_1(2)$], pertinent to our rotational temperature determinations. This value follows from the recently updated line parameters for the Meinel system of the OH radical.[31] In addition, the $P_1(2)$ intensities are corrected for Q(5) contamination which is estimated to be $\cong 2\%$ at a temperature of 200 K. Comparisons of the MTM temperatures with those obtained by other well calibrated instruments (Na temperature lidars and FTIR spectrometers) indicate that our absolute temperatures are reliable to ±5 K. However, the precision of the measurements (most important for determining wave perturbation amplitudes) is much higher at ~2 K in 3 min (or ~0.5 K in 30 min).

Since the development of the MTM in 1996, it has been used in two extended series of measurements to investigate gravity wave characteristics and mesospheric temperature variability over the Rocky Mountains. The first seasonal measurements were made from Ft. Collins, Colorado (41°N, 105°W) where it was operated alongside a Na temperature lidar (C.Y. She, Colorado State University) for a one-year period (June 1997 – June 1998). More recently, the MTM was operated at the Starfire Optical Range, New Mexico (35°N, 107°W) from October 1998-December 1999, where it provided data as part of a cluster of instruments, which included a Na wind/temperature lidar (C.S. Gardner, University of Illinois) and a meteor radar (W. Hocking, University of Western Ontario, Canada). In October 2001 the MTM was moved to the U.S. Air Force Maui Optical Station (AMOS) on Haleakala Crater, Maui, Hawaii for long-term coordinated measurements as part of an instrument cluster, under the joint NSF/AFOSR (Air Force Office of Scientific Research) sponsored Maui-MALT initiative.

Fig. 6. Example of MTM data obtained from Ft. Collins, Colorado showing a well-defined long-period oscillation (~9.2-hr) evident in OH M(6,2) band intensity (Fig. 6a) and rotational temperature (Fig. 6b). Superimposed on both plots is a coherent short-period (~40 min) gravity wave.
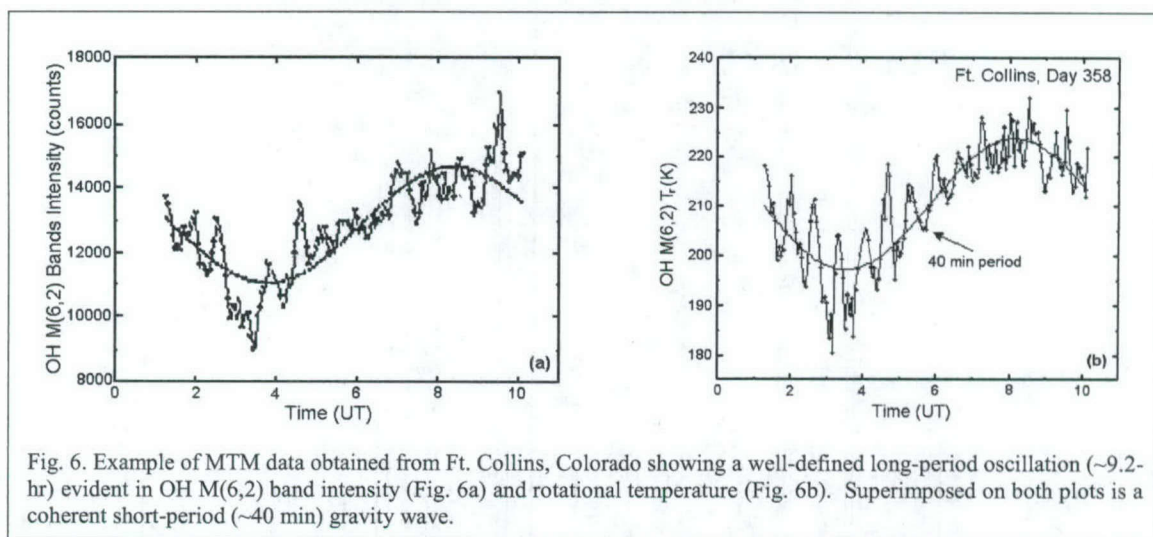
Figure 6a,b is an example of the MTM temperature data from Ft. Collins showing a well-defined short-period (~40 min) oscillation in the OH rotational temperature and band intensity superimposed on a large amplitude, long period (~ 9.2-hr) oscillation. In this case the intensity and temperature of the large-scale wave are approximately in phase, however on other occasions a marked phase shift is observed. Analysis of similar data obtained over and extended 10-day period during the autumn of 1996 suggests the longer period wave is the result of the terdiurnal (~8-hr) tidal oscillation.[32] By combining the amplitude of the relative intensity ($\Delta I/I$ ~22%) and temperature ($\Delta T/T$ ~5.5%) perturbations with the observed phase shift and comparing with model results for the Krassovsky ratio, (the ratio of $\Delta I/I$ to $\Delta T/T$) [e.g. [33, 34]], the origin of such waves (i.e. tidal or inertial gravity wave) can be investigated further. In comparison, the shorter period (~40 min) waves exhibit significantly smaller perturbation amplitudes (ΔI ~5-10% and ΔT ~5-8 K) that are nevertheless clearly resolvable at the resolution of the MTM data (~3 min and ~1.5 K). Such events are numerous in our collaborative data sets but have yet to be investigated in detail.

An enhanced capability for the MTM was recently implemented as part of an upgrade for the NSF/NASA CEDAR-TIMED program enabling measurements of both OH and O_2 temperatures as a function of time. This technique has been used previously by Hecht and Walterscheid [35] to study large-scale waves observed during the ALOHA Campaigns. Figure 7 illustrates this new capability which enables the amplitude and phase of long and short period waves to be investigated at two centroid altitudes (~87 and 94 km) within the MLT. In this example, a long period (~11-hr) oscillation and a superposed shorter period wave (~80 min) are evident in both emissions. The data were obtained from BLO on 1/2 December 2000. For clarity, only the temperature data are plotted here. A marked phase shift exists between the two large amplitude waves with the O_2 signal leading the OH indicative of a downward progressing semi-diurnal tide. The same signatures are evident in the respective band intensity data (not shown) which also yield information on the relative phase relationships between the intensity and temperature waves and their amplitudes. The ability to measure the temperature perturbations ($\Delta T/T$) as well as the intensity variations ($\Delta I/I$) induced by the passage
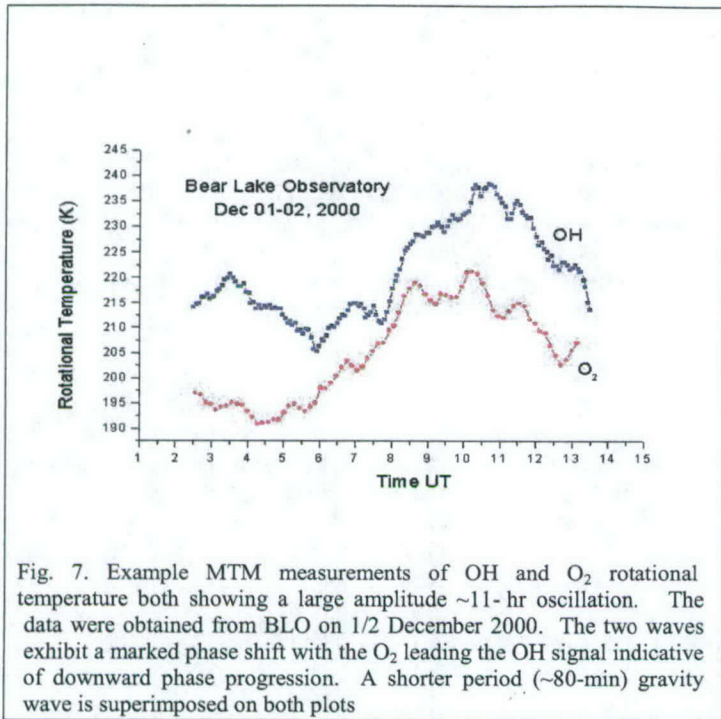
Fig. 7. Example MTM measurements of OH and O_2 rotational temperature both showing a large amplitude ~11- hr oscillation. The data were obtained from BLO on 1/2 December 2000. The two waves exhibit a marked phase shift with the O_2 leading the OH signal indicative of downward phase progression. A shorter period (~80-min) gravity wave is superimposed on both plots

of monochromatic gravity waves provides a new method for estimating their momentum flux, when combined with information on their intrinsic wave parameters.

Finally, Figure 8 compares MTM data with University of Illinois Na wind/temperature lidar data obtained recently from Haleakala Crater, Maui, Hawaii as part of the Maui-MALT initiative. The left hand box in this figure shows the lidar measurements of mesospheric temperature as a function of altitude (~80-105 km) and UT time for the night of 11 April 2002. A strong descending tidal oscillation is evident throughout the night creating temperature variations of over 40 K. The corresponding OH and O_2 MTM data are plotted on the right side of the figure together with the height averaged Na lidar data (using Gaussian profiles centered on 87 and 94 km, respectively, with a FWHM ~10 km). The agreement between the two data sets is quite remarkable when it is considered that the two instruments use quite different techniques to derive the mesospheric temperature. As the MTM operates unattended and obtains data on typically 22 nights/month (weather permitting) these measurements can be used to extend considerably the coverage provided by lidar measurements. Such studies are of key importance for seasonal climatology studies focusing on the effects of shorter-term variations associated with seasonal transitions and planetary waves that are not yet included in current global-scale atmospheric models.
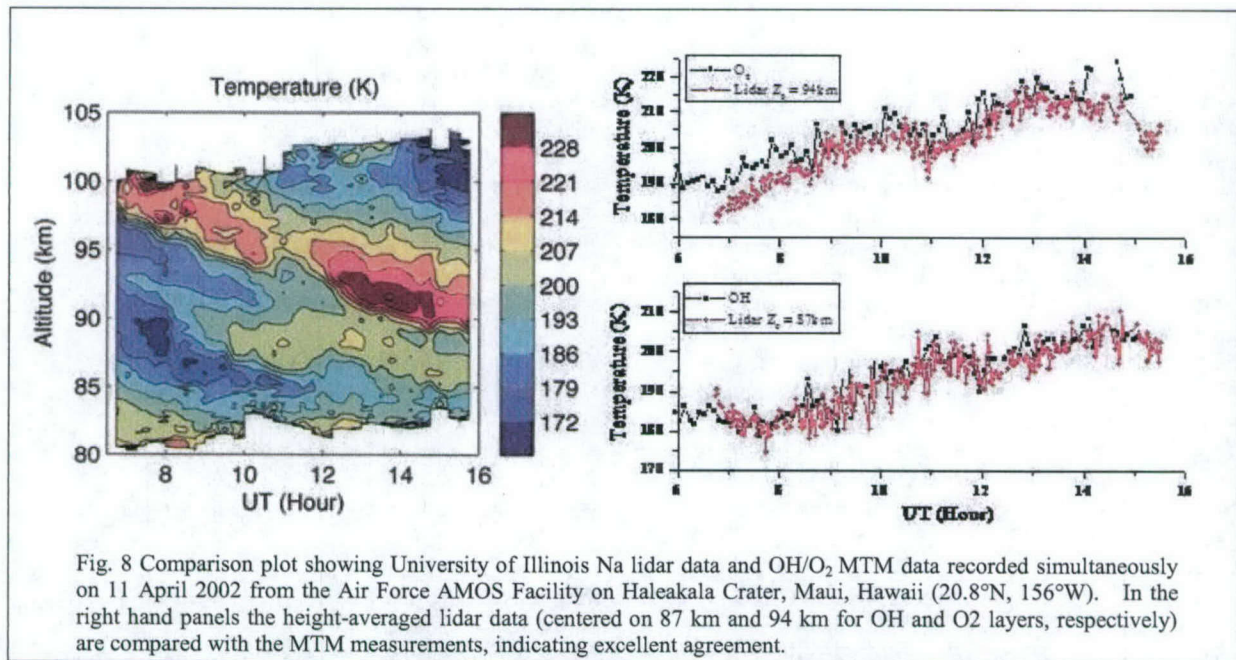

Fig. 8 Comparison plot showing University of Illinois Na lidar data and OH/O_2 MTM data recorded simultaneously on 11 April 2002 from the Air Force AMOS Facility on Haleakala Crater, Maui, Hawaii (20.8°N, 156°W). In the right hand panels the height-averaged lidar data (centered on 87 km and 94 km for OH and O2 layers, respectively) are compared with the MTM measurements, indicating excellent agreement.

6. CONCLUSIONS

Image measurements of the nightglow emissions, which were once considered a novelty, have now proven to be an essential element in the quantitative investigation of gravity wave forcing of the MLT region [e.g. [36-38]]. In particular their sensitivity to small-scale waves as well as their adaptability to multi-wavelength radiance and temperature measurements makes them a powerful tool for dynamical studies. The two-dimensional image data provide a direct measure of wave anisotropy, important for investigating wind filtering and ducting effects as well as novel data on wave breaking and turbulence leading to the transfer of momentum into the background flow [e.g. [39]].

Ongoing observations as part of the NSF/NASA CEDAR-TIMED collaborative program and the NSF/AFOSR Maui-MALT initiative will provide important new data on seasonal variability of gravity waves and their sources over two physically distinct source regions. In particular, the "image chain" measurements over the Rocky Mountains are well suited for investigating the effects of gravity wave propagation and dissipation in the presence of potentially strong orographic forcing. Analysis of these new data will enable a much more detailed study of wave geographical extent and azimuthal anisotropy than has previously been possible. In comparison, clustered Maui-MALT measurements from the Hawaiian Islands, which are located centrally in the Pacific Ocean (21°N, 156°W) over 3000 km from any substantial land mass (except the islands themselves), are expected to be controlled by convective-type weather disturbances.

7. ACKNOWLEDGEMENTS

8. REFERENCES

1. Leovy, C., Simple models of thermally driven mesospheric circulation, *J. Atmos. Sci., 21*, 327, 1964.
2. Lindzen, R.S., Wave-mean flow interactions in the upper atmosphere, *Boundary-Layer Met., 4*, 327-343, 1973.
3. Holton, J.R., The influence of gravity wave breaking on the circulation of the middle atmosphere, *J. Atmos. Sci., 40*, 2497-2507, 1983.
4. Garcia, R.R., and S. Solomon, The effect of breaking gravity waves on the dynamics and chemical composition of the mesosphere and lower thermosphere, *J. Geophys. Res., 90*, 3850, 1985.
5. Fritts, D.C., and R.A. Vincent, Mesospheric momentum flux studies at Adelaide, Australia: Observations and gravity wave-tidal interaction model, *J. Atmos. Sci., 44*, 605, 1987.
6. States, R. J., and C. S. Gardner, Thermal structure of the mesopause region (80-105 km) at 40°N latitude. Part II: diurnal variations, *J. Atmos. Sci., 57*, 78-92, 2000.
7. She, C. Y., S. S. Chen, Z. L. Hu, J. Sherman, J. D. Vance, V. Vasoli, M. A.White, J. R. Yu, and D. A. Krueger, Eight-year climatology of nocturnal temperature and sodium density in the mesopause region (80 to 105 km) over Fort Collins, CO (41°N, 105°W), *Geophys. Res. Lett., 27*, 3289 - 3292, 2000.
8. Seo, S-H., All-sky measurements of the mesospheric "frontal events" from Bear Lake Observatory, Utah, M.Sc. Thesis, Physics Department, Utah State University, 1998.
9. Swenson, G.R., and S.B. Mende, OH emission and gravity waves (including a breaking wave) in all-sky imagery from Bear Lake, UT, *Geophys. Res. Lett., 21*, 2239, 1994.
10. Taylor, M.J., M.B. Bishop and V. Taylor, All-sky measurements of short period waves imaged in the OI(557.7 nm), Na(589.2 nm) and near infrared OH and $O_2(0,1)$ nightglow emissions during the ALOHA-93 campaign. *Geophys. Res. Lett., 22*, 2833, 1995c.
11. Taylor, M.J., D.N. Turnbull, and R. P. Lowe, Spectrometric and imaging measurements of a spectacular gravity wave event observed during the ALOHA-93 Campaign. *Geophys. Res. Lett., 22*, 2849, 1995a.

12. Taylor, M.J., D.C. Fritts and J.R. Isler, Determination of horizontal and vertical structure of a novel pattern of short period gravity waves imaged during ALOHA-93, *Geophys. Res. Lett., 22*, 2837, 1995b.

13. Taylor, M.J., Y.Y. Gu, X. Tao, C.S. Gardner and M.B. Bishop, An investigation of intrinsic gravity wave signatures using coordinated lidar and nightglow image measurements. *Geophys. Res. Lett., 22*, 2853, 1995d.

14. Wu, Q., and T.L. Killeen, Seasonal dependence of mesospheric gravity waves (<100 km) at Peach Mountain Observatory, Michigan, *Geophys. Res. Lett., 23*, 2211-2214, 1996.

15. Hecht, J.H., R.L. Walterscheid, D.C. Fritts, J.R. Isler, D.C. Senft, C.S. Gardner, and S. J. Franke, Wave breaking signatures in OH airglow and sodium densities and temperatures. 1, Airglow imaging, Na lidar, and MF radar observations, *J. Geophys. Res., 102*, 6655-6668, 1997.

16. Fritts, D.C., Gravity wave forcing and effects in the mesosphere and lower thermosphere, in *The Upper Mesosphere and Lower Thermosphere: A Review of Experiment and Theory*, Geophysical Monograph 87, R.M. Johnson and T.L. Killeen eds., American Geophysical Union, Washington, D.C., 1995.

17. Taylor, M.J., and M.A. Hapgood, On the origin of ripple type wave structure in the OH nightglow emission, *Planet. Space Sci., 35*, 1421, 1990.

18. Dewan, E.M., and R.H. Picard, Mesospheric bores, *J. Geophys. Res., 103*, 6295-6305, 1998.

19. Taylor, M.J., W.R. Pendleton, Jr., S. Clark, H. Takahashi, D. Gobbi, and R.A. Goldberg, Image measurements of short-period gravity waves at equatorial latitudes, *J. Geophys. Res., 102*, 26283, 1997.

20. Taylor, M.J., E.H. Ryan, T.F. Tuan, and R. Edwards, Evidence of preferential directions for gravity wave propagation due to wind filtering in the middle atmosphere, *J. Geophys. Res., 98*(A4), 6047, 1993.

21. Zhong, L., A.H. Manson, L.J. Sonmor, and C.E. Meek, Gravity wave exclusion circles in background flows modulated by the semidiurnal tide, *Ann. Geophys., 14*, 557, 1996.

22. Medeiros, A.F., M.J. Taylor, H. Takahashi, P.P. Batista, and D. Gobbi. An investigation of gravity wave activity in the low-latitude upper mesosphere: Propagation direction and wind filtering, *J. Geophys. Res.*, in review, October 2002.

23. Nakamura, T., A. Higashikawa, T. Tsuda, and Y. Matsushita, Seasonal variations of gravity wave structures in OH airglow with a CCD imager at Shigaraki, *Earth Planets Space, 51*, 897-906, 1999.

24. Walterscheid. R.L., J.H. Hecht, R.A. Vincent, I.M. Reid, J. Woithe, and M.P. Hickey, Analysis and interpretation of airglow and radar observations of quasi-monochromatic gravity waves in the upper mesosphere and lower thermosphere over Adelaide, Australia (35°S, 138°E), *J. Atmos. Solar-Terr. Phys., 61*, 461-478, 1999.

25. Hecht, J.H., R.L. Walterscheid, M.P. Hickey and S.J. Franke, Climatology and modeling of quasi-monochromatic atmospheric gravity waves observed over Urbana, Illinois, *J. Geophys. Res., 106*, 5181-5195, 2001.

26. Tuan, T.F., and D. Tadic, A dispersion formula for analyzing 'modal interference' among guided and free gravity wave modes and other phenomena in a realistic atmosphere, *J. Geophys. Res., 87*, 1648, 1982.

27. Chimonas, G., and C.O. Hines, Doppler ducting of atmospheric gravity waves, , *J. Geophys. Res., 91*, 1219, 1986.

28. Isler, J.R., M.J. Taylor and D.C. Fritts, Observational evidence of wave ducting in the mesosphere, *J. Geophys. Res., 102*, 26301, 1997. 29. Dewan, E.M., and R.H. Picard, On the origin of mesospheric bores, *J. Geophys. Res., 106*, 2921-2927, 2001.

29. Dewan, E.M., and R.H. Picard, On the origin of mesospheric bores, *J. Geophys. Res., 106*, 2921-2927, 2001.

30. Meriwether, J. W., High latitude airglow observations of correlated short-term fluctuations in the hydroxyl Meinel 8-3 band intensity and rotational temperature, *Planet. Space Sci., 43*, 1211-1221, 1975.

31. Goldman, A., W. G. Schoenfeld, D. Goorvitch, C. Chackerian Jr., H. Dothe, F. Mélen, M. C. Abrams, and J. E. A. Selby, Updated line parameters for the OH $X^2\Pi$-$X^2\Pi$ (v",v') transitions, *J. Quant. Spectrosc. Radiat. Transfer, 59*, 453-469, 1998.

32. Pendleton, W.R., Jr., M.J. Taylor, and L.C. Gardner, Terdiurnal oscillations in OH Meinel rotational temperatures for fall conditions at northern mid-latitude sites, *Geophys. Res. Lett., 27*, 1799-1802, 2000.

33. Gardner, L.C., Krassovsky's ratio for long period waves for the OH M(6,2) intensity and rotational temperature using the CEDAR Mesospheric Temperature Mapper, M.Sc. Thesis, Physics Department, Utah State University, 2000.

34. Taylor, M.J., L.C. Gardner, and W.R. Pendleton, Jr., Long-period wave signatures in mesospheric OH Meinel (6,2) band intensity and rotational temperature at mid-latitudes, *Adv. Space Res., 27*, 1171-1179, 2001.

35. Hecht, J.H., and R.L. Walterscheid, Observations of the OH Meinel (6,2) and O_2 Atmospheric (0,1) nightglow emissions from Maui during the ALOHA-90 campaign, *Geophys. Res. Lett., 18*, 1441, 1991.

36. Swenson, G.R., and A.Z. Liu, A model for calculating acoustic gravity wave energy and momentum flux in the mesosphere from OH airglow, *Geophys. Res. Lett., 25*, 477, 1998.

37. Swenson, G.R., R. Haque, W. Yang, and C. S. Gardner, Momentum and energy fluxes of monochromatic gravity waves observed by an OH imager at Starfire Optical Range, NM, , *J. Geophys. Res., 104,* 6067, 1999.
38. Fritts, D.C., S.L. Vadas, and Y. Yamada, An estimate of strong local body forcing and gravity wave radiation based on OH airglow and meteor radar observations, *Geophys. Res. Lett., 29*, 71-74, 2002.
39. Yamada, Y., H. Fukunishi, T. Nakamura, and T. Tsuda, Breaking of small-scale gravity wave and transition to turbulence observed in OH airglow, *Geophys. Res. Lett., 28*, 2153-2156, 2001.
40. Taylor, M.J., and W.R. Pendleton, Jr., Buoyancy and buoyancy waves: Optical observations, in *Encyclopedia of Atmospheric Sciences*, J.R. Holton, J. Pyle, and J.A. Curry, eds., Academic Press, San Diego, 2002.